Available online at www.sciencedirect.com
ScienceDirect
International Journal of Heat and Mass Transfer 50 (2007) 2107–2116
International Journal of HEAT and MASS TRANSFER
www.elsevier.com/locate/ijhmt

# Experimental and numerical investigation of downward gas-dispersed turbulent pipe flow

M.A. Pakhomov [a], M.V. Protasov [b,1], V.I. Terekhov [a,*], A.Yu. Varaksin [b,1]

[a] *Kutateladze Institute of Thermophysics, Siberian Division, Russian Academy of Sciences, Novosibirsk, 630090, Russia*
[b] *Institute of High Temperatures, Russian Academy of Sciences, Moscow 125412, Russia*

Received 10 October 2006; received in revised form 25 October 2006
Available online 12 January 2007

**Abstract**

Results of experimental and numerical simulations of the downward turbulent gas flow laden with dispersed solid particles in a vertical pipe are presented. The influence of the particles on the turbulence was studied at moderate particle concentrations. The radial profiles of the axial and radial velocity components and of the turbulent kinetic energy of the carrier (gas) and the dispersed phases (50 μm spherical glass particles) were measured using two-component laser Doppler anemometer (LDA). Calculations were performed at both experimental and superset conditions with various size and material of particles. The mathematical formulation employs a set of equations in Euler variables for description of the transport processes in the fluid and disperse phases. The addition of particles into a turbulent carrier flow decreases the level of turbulence of the gas phase because of particles involvement into fluctuation motion. A significant anisotropy of fluctuations of the particle velocity is found. The amplitude of turbulent fluctuations of particle velocity in the axial direction is much higher than that in the radial direction.


*Keywords:* Dispersed flow; Turbulence modification; Measurements; Simulation

## 1. Introduction

Dispersed two-phase turbulent flows are widely encountered in both environmental and engineering field. Numerous natural atmospheric gas-dispersed (air-particle) flows include sand, dust and rain storms, tornados, smog, smoke. Gas flows laden with solid particles or droplets occur in many industrial applications such as gas cleaning and pneumatic transport systems, different power-generating facilities.

Particle-laden flow is a complex system with behavior determined by many factors intervening. In turbulent multiphase flows all phases can be in slip and fluctuating motion and interactions between the phases are very complicated. The full two-way coupling of the turbulent fluctuations must be taken into account because even a small loading of the disperse phase to single-phase flow can greatly affect the characteristics of the continuous phase and cause cardinal changes in the flow pattern. This is associated, first of all, with the diversity of the properties of disperse phase, resulting in versatile modes of dispersed two-phase gas-dispersed flows. A change in concentration and size of particles may lead to both quantitative and qualitative restructuring of flow (for example, to earlier laminar-turbulent transition or, on the contrary, to laminarization of flow).

Development of methods for the simulation of two-phase gas-dispersed flows is one of the most complex problems in the present-day fluid mechanics. Nevertheless, the extensive use of gas-dispersed flows for practical applications has stimulated numerous investigations of

* Corresponding author. Tel.: +7 3833 306 736; fax: +7 3833 308 480.
*E-mail addresses:* pakhomov@ngs.ru (M.A. Pakhomov), protasov_m@mail.ru (M.V. Protasov), terekhov@itp.nsc.ru (V.I. Terekhov), varaksin_a@mail.ru (A.Yu. Varaksin).
[1] Tel.: +7 4954 858 090; fax: +7 4954 853 081.

0017-9310/$ - see front matter © 2006 Elsevier Ltd. All rights reserved.
doi:10.1016/j.ijheatmasstransfer.2006.11.009

**Nomenclature**

$C_D$ drag coefficient
$D_{xP}$, $D_{rP}$ coefficients of turbulent diffusion of particles in the axial and radial directions, $m^2/s$
$d$ particle diameter, m
$g$ acceleration of gravity, $m/s^2$
$g_k$, $g_\varepsilon$ coefficients of involvement of particles (response to) into microfluctuation motion of the gas phase
$k$ turbulence kinetic energy, $m^2/s^2$
$L$ mixing length, m
$M_P$ mass loading ratio
$P$ pressure, Pa
$\Re$ gas constant, J/(mol K)
$R$ pipe radius, m
$Re$ Reynolds number of flow
$Re_P = \rho d\sqrt{(U-U_P)^2+(V-V_P)^2}/\mu$ Reynolds number of particle
$Re_T = k^2/(\varepsilon v)$ turbulence Reynolds number
$Stk$ Stokes number in the large-scale fluctuation motion
$T$ temperature, K
Tu turbulence intensity
$U$, $V$ mean velocity in axial and radial directions, m/s
$\langle uv\rangle = -v_T(\partial U/\partial r)$ turbulent stresses in gas, $m^2/s^2$
$\langle u_P v_P\rangle$ turbulent stresses in the dispersed phase, $m^2/s^2$
$\langle u^2\rangle$, $\langle v^2\rangle$ mean-square fluctuation velocities in the axial and radial directions, $m^2/s^2$
$U_*$ friction velocity, m/s
$W = (1 + Re_P^{2/3}/6)$ correction function (Reynolds number correction factor)
$w_t$, $w_n$ particle momentum recovery factors in the tangential and normal directions to the channel wall
$x$, $r$ axial and radial coordinates, m
$y$ distance from the wall, m

*Greek symbols*
$\varepsilon$ dissipation rate of turbulence kinetic energy, $m^2/s^3$
$\Phi$ volume concentration of particles
$\Gamma^E = v_T/\langle u^2\rangle$ turbulent scale of gas
$\mu$ dynamic viscosity, (N s)/$m^2$
$v$ kinematic viscosity, $m^2/s$
$\Omega^\varepsilon = (15v/\varepsilon)^{1/2}$ time microscale, s
$\Omega^E$ Eulerian time macroscale, s
$\Omega^L$ Lagrangian time macroscale, s
$\Omega^{\varepsilon L}$ time of interaction between particle and energy-carrying eddies, s
$\rho$ density, $kg/m^3$
$\tau = \rho_P d^2/(18\ \mu W)$ particle dynamic relaxation time, s

*Subscripts*
0 parameter on the pipe axis
1 parameter at the inlet
A unladen air flow
$i$ current calculation in the axial direction
$i-1$ preceding calculation in the axial direction
P particle
T parameter of turbulence
W parameter on the wall
$+$ dimensionless parameters in the wall coordinates

*Symbol*
$\langle\,\rangle$ ensemble average

*Acronym*
DNS direct numerical simulation
LES large-eddy simulation
LDA laser doppler anemometry
LRN low-Reynolds-number
PDF probability density function
PIV particle image velocimetry

hydromechanics of flows with solid particles. Some of known numerous recent generalizing studies are given in the list of references [1–10]. At the same time, number of important aspects of two-phase flows, have been studied inadequately, and the experimental data and physical models developed so far are fragmentary and often contradictory.

This explains importance of detailed experimental studies and development a valid mathematical models for description of such flows.

The purpose of the present paper is the experimental and numerical investigation of the structure of downward turbulent gas-dispersed flows in a vertical pipe at moderate loading ratios $M_P < 0.35$.

## 2. Experimental set-up

Simultaneous measurements of tracers and particles were carried out with the experimental setup (described in detail in [10]) of the particle laden downward turbulent pipe flow at constant Reynolds number $Re = 15{,}300$. Spherical glass particles having an average diameter of 50 μm (root-mean-square deviation −5 μm) and density −2550 $kg/m^3$ were used as dispersed phase. The distance

from the particles entrance section to the measuring cross-section was equal 1380 mm. The facility operates in an open (with respect to gas and dispersed phase) circuit. This scheme enables one to assurance determine the cross to pipe average concentration (gas-to-solid mass loading ratio) of the dispersed phase with the desired accuracy through direct independent measurements of the flow rates of the gas and solid particles. The use of an open circuit further is valuable in easy control of the flow rates of both gas and dispersed phases. Particle mass loading is defined as the ratio of the mass of particles to the mass of the fluid phase in the flow.

The test section was a 2500 mm long vertical pipe of stainless steel with inner diameter of $2R = 46$ mm. A slit 12 mm wide for the inlet and outlet of probing beams of a two-component laser Doppler anemometer (LDA 10 by Dantec, Denmark) was milled in the wall at the distance of 1380 mm ($x/2R = 30$) from the particle entrance section. Air was delivered into the test section from compressed-air flasks via the receiver and pressure regulator providing a constant gas flow rate (±1%). A particle two-liter feeder was mounted above the entrance of the pipe. In order to obtain a gas-dispersed flow, a constant particle mass flow rate is fed into the air pipe flow by a particle feeder system. The particles were taken up by the air flow, carried to the test section, and were deposited in a gravitational chamber. Tracer particles with a size in the range 2–3 μm were introduced into the flow for measurements of the carrier phase velocity; a Dantec-made seeding generator was used for this purpose. The pipe cross section was scanned using a 57H00 traverse system by Dantec.

## 3. Formulation of the problem

The mathematical formulation of the problem and its numerical realization largely correspond to the model developed in [11,12]. The main improvement is that here we have performed a calculation of a turbulent isothermal pipe gas–solid flow taking into account the collisions of particles with the pipe wall. The dispersed phase motion is simulated within the Eulerian approach and largely corresponds to the numerical model developed in [12]. The Eulerian approach is advantageous over the combined Eulerian–Lagrangian description in that one type of equations is used for description of the transport processes in the gas and dispersed phases. In addition, the description of transport of tiny particles creates no problems because here we deal with a limiting transition to the case of zero-mass impurity diffusion.

The volume concentration of the dispersed phase is low ($\Phi < 10^{-4}$), and the particles are quite small (diameter $d < 200$ μm). In the case of a two-phase flow, the particle collisions may be ignored for a volume concentration of the dispersed phase of $\Phi < 10^{-3}$ (according to the data of Volkov et al. [7]). We assume that the particles interact with the confining surface ignoring the effect of slipping and rotation after the collisions.

## 4. The set of basic equations

### 4.1. Gas phase

The set of continuity and momentum equations describing the gas phase motion within a two-phase gas-dispersed flow in the boundary layer approximation takes the form

$$\begin{aligned}
&\frac{\partial U}{\partial x}+\frac{1}{r}\frac{\partial (rV)}{\partial r}=0\\
&\rho\left[U\frac{\partial U}{\partial x}+\frac{V}{r}\frac{\partial (rU)}{\partial r}\right]=-\frac{\partial P}{\partial x}+\frac{1}{r}\frac{\partial}{\partial r}\left[r(\mu+\mu_{\mathrm{T}})\frac{\partial U}{\partial r}\right]\\
&\qquad\qquad -\frac{3}{4d}C_{\mathrm{D}}\rho\Phi(U-U_{\mathrm{P}})|\vec{U}-\vec{U}_{\mathrm{P}}|\\
&\rho=P/(\Re T).
\end{aligned}\tag{1}$$

The equation for the gas phase motion has an additional term responsible for interphase dynamic interaction.

### 4.2. Two-parameter k–ε model of turbulence

The turbulent characteristics of the fluid phase are calculated using the Nagano–Tagawa LRN $k$–$\varepsilon$ turbulence model (1990) [13], modified for the case of dispersed phase presented. The transport equations for the kinetic energy of turbulence $k$ and for its dissipation rate $\varepsilon$, modified for the case of presence of the dispersed phase, have the form

$$\rho\left[U\frac{\partial k}{\partial x}+\frac{V}{r}\frac{\partial (rk)}{\partial r}\right]=\frac{1}{r}\frac{\partial}{\partial r}\left[\left(\mu+\frac{\mu_{\mathrm{T}}}{\sigma_k}\right)\frac{\partial k}{\partial r}\right]+\Pi-\rho\varepsilon+S_k \tag{2}$$

$$\begin{aligned}
\rho\left[U\frac{\partial \varepsilon}{\partial x}+\frac{V}{r}\frac{\partial (r\varepsilon)}{\partial r}\right]&=\frac{1}{r}\frac{\partial}{\partial r}\left[r\left(\mu+\frac{\mu_{\mathrm{T}}}{\sigma_\varepsilon}\right)\frac{\partial \varepsilon}{\partial r}\right]\\
&\quad+\frac{\varepsilon}{k}(C_{\varepsilon 1}f_1\Pi-C_{\varepsilon 2}\varepsilon\rho f_2)+S_\varepsilon.
\end{aligned}\tag{3}$$

The constants and damping functions have the form [13]

$$C_\mu=0.09;\quad \sigma_k=1.4;\quad \sigma_\varepsilon=1.3;$$

$$C_{\varepsilon 1}=1.45;\quad C_{\varepsilon 2}=1.9;\quad f_1=1;\quad \Pi=\mu_{\mathrm{T}}\left(\frac{\partial U}{\partial r}\right)^2;$$

$$f_2=[1-\exp(-y_+/6)]^2[1-0.3\exp\{-(Re_{\mathrm{T}}^{3/4}/6.5)^2\}];$$

$$f_\mu=[1-\exp(-y_+/26)]^2(1+4.1/Re_{\mathrm{T}}^{3/4}).$$

The coefficient of turbulent viscosity $\mu_{\mathrm{T}}$ and turbulent stresses of gas phase are calculated within the two-parameter $k$–$\varepsilon$ model,

$$\mu_{\mathrm{T}}=C_\mu f_\mu\rho k^2/\varepsilon;\quad \langle uv\rangle=-\nu_{\mathrm{T}}\frac{\partial U}{\partial r}.$$

The terms, which characterize additional dissipation of turbulence energy and exchange of energy with averaged motion in Eq. (2), are determined according to Volkov et al. [7],

$$S_k=\underbrace{-\frac{2M_{\mathrm{P}}\rho k}{\tau}\exp(-\Omega^{\mathrm{L}}/\tau)}_{\mathrm{I}}\underbrace{-g_k\mu_{\mathrm{T}}(U-U_{\mathrm{P}})\frac{\partial U}{\partial x}\frac{\partial M_{\mathrm{P}}}{\partial x}}_{\mathrm{II}}. \tag{4}$$

Here, the term (I) denotes the additional dissipation of turbulent energy due to because of the presence of small particles, and (II) denotes the energy exchange with averaged motion through averaged interphase slip at a nonuniform distribution of particle concentration.

The terms, which characterize the effect of small particles on the rate of dissipation of turbulent energy of gas and the opposite effect on turbulence in Eq. (3) (see [7])

$$S_\varepsilon = \underbrace{-\frac{2M_P\rho_P\varepsilon}{\tau}\exp(-\Omega^\varepsilon/\tau)}_{\mathrm{I}} + \underbrace{\frac{2}{3}g_\varepsilon\rho\varepsilon\left[(U-U_P)\frac{\partial M_P}{\partial x}+(V-V_P)\frac{\partial M_P}{\partial r}\right]}_{\mathrm{II}}, \quad (5)$$

where (I) denotes the effect of small particles on the rate of turbulent energy dissipation of carrier flow, and (II) denotes the inverse effect of particles on the turbulence due to the averaged slip and nonuniform distribution of the dispersed phase.

We use the relation suggested by Simonin et al. [14] to calculate the time macroscale of turbulence $\Omega^E$ in the core region of flow. The integral Eulerian scale of turbulence for gas in the near wall region is determined by the relation given by Derevich [15],

$$\Omega^E_+ = \Omega^E U_*/\nu = \sqrt{\left(\Omega^E_+\right)^2_0 + \left(\Omega^E_+\right)^2_W}; \quad \left(\Omega^E_+\right)_W \approx 10.$$

The correlation between the Lagrangian $\Omega^L$ and Eulerian $\Omega^E$ time scales of turbulence for small particles has the form $\Omega^L \approx 0.608\Omega^E$ [15].

The relations for axial and radial velocity fluctuations of gas are likewise borrowed from Derevich [15].

The coefficients of involvement of particles into turbulent motion of gas flow in Eqs. (4) and (5) have the form [7,15]

$$g_k = \Omega^{\varepsilon L}/\tau - 1 + \exp(-\Omega^{\varepsilon L}/\tau);$$
$$g_\varepsilon = \Omega^\varepsilon/\tau - 1 + \exp(-\Omega^\varepsilon/\tau).$$

Here, $\Omega^\varepsilon = (15\nu/\varepsilon)^{1/2}$ is the Eulerian time microscale of turbulence. The time of interaction between a particle and energy-carrying eddies of the gas phase $\Omega^{\varepsilon L}$ is determined by the relations [15]

$$\Omega^{\varepsilon L} = \begin{cases} \Omega^\varepsilon, & |\vec{U}-\vec{U}_P|\Omega^\varepsilon \leqslant \Gamma^E \\ \Gamma^E/|\vec{U}-\vec{U}_P|, & |\vec{U}-\vec{U}_P|\Omega^\varepsilon > \Gamma^E \end{cases}, \quad (6)$$

where $\Gamma^E = \nu_T/\langle u^2\rangle$ is the geometric scale of turbulence of the carrier phase, and $\tau = \rho_P d^2/(18\,\mu W)$ is the dynamic relaxation time of particles.

### 4.3. Dispersed phase

One of the methods of constructing the set of equations for the description of processes of momentum transfer in the dispersed phase is that of using a kinetic equation for the probability density function (PDF) for the particle velocity in a turbulent flow. The equation for PDF is derived on the assumption that the emergence of velocity fluctuations of the dispersed phase is caused by the interaction between particles and turbulent fluctuations of gas which are modeled by Gaussian random functions. The simulation of a real turbulent flow by Gaussian process is an approximate method; however, this method brings satisfactory practical results. An equation of probability density of particle distribution by coordinates, velocity, and temperature in turbulent flow [7,15] is introduced for transition from a dynamic stochastic equation describing the paths of individual particles of the Langevin type to a continuous simulation of the ensemble of the dispersed phase. The kinetic equation for PDF may yield a set of equations for simulation of the dynamics and heat transfer of the dispersed phase in the Eulerian continuous approach (see, for example, [4,7–9,11,12,14–16]).

Numerous recent studies [7–9,14–17] reveal that, for the conditions examined in this paper, the main forces acting on a particle in turbulent flow are the forces of turbophoresis, aerodynamic drag, and gravity. The results of DNS and LES calculations [16] were used to demonstrate that the transport of small particles is largely affected by the gas turbulence and inertial forces. The effect of the Magnus and Saffman forces and of the force due to pressure gradient, as well as the associated mass and Basset effects, are ignored in view of their smallness.

The Derevich model (2002) [15] is used to determine the velocity components of the dispersed phase and the mean-square values of the particle velocity distribution. The set of equations of transport of the dispersed phase in cylindrical coordinates for the axisymmetric case has the form

$$\frac{\partial(\Phi U_P)}{\partial x}+\frac{1}{r}\frac{\partial(r\Phi V_P)}{\partial r}=0$$
$$\underbrace{U_P\frac{\partial U_P}{\partial x}+\frac{V_P}{r}\frac{\partial(rU_P)}{\partial r}}_{\mathrm{I}}+\underbrace{\frac{\partial\langle v_P^2\rangle}{\partial x}}_{\mathrm{II}}+\underbrace{\frac{1}{r\Phi}\frac{\partial}{\partial r}[r\Phi\langle u_P v_P\rangle]}_{\mathrm{III}}$$
$$=\underbrace{\frac{U-U_P\pm\tau g}{\tau}}_{\mathrm{IV}}-\underbrace{\frac{D_{xP}}{\tau}\frac{\partial(\ln\Phi)}{\partial x}}_{\mathrm{V}} \quad (7)$$
$$\underbrace{U_P\frac{\partial V_P}{\partial x}+\frac{V_P}{r}\frac{\partial(rV_P)}{\partial r}}_{\mathrm{I}}+\underbrace{\frac{\partial\langle v_P^2\rangle}{\partial r}}_{\mathrm{II}}$$
$$=\underbrace{\frac{V-V_P}{\tau}}_{\mathrm{IV}}-\underbrace{\frac{D_{rP}}{\tau}\frac{\partial(\ln\Phi)}{\partial r}}_{\mathrm{V}}+\underbrace{\frac{2}{3}\frac{k}{r}(1+\tau/\Omega^L)^{-1}}_{\mathrm{VI}}.$$

The axial and radial transport of particles is due to the effect of the following force factors: (I), convection of momentum; (II), the force of turbophoresis caused by the nonuniformity of turbulent energy of the dispersed phase; (III), the term responsible for the correlations of fluctuations of the axial and radial components of particle velocity; (IV), the force of aerodynamic drag; (V), the diffusion travel of particles due to the gradient of their concentra-

tion; and (VI), the term which allows for the effect of the azimuthal component of velocity of disperse phase on the particle transport.

Here, $\langle u_P v_P \rangle$ denotes the correlation of fluctuations of the axial and radial components of particle velocities (turbulent stresses in the dispersed phase) and is written as [15]

$$\langle u_P v_P \rangle = \underbrace{q_P \langle uv \rangle}_{I} - \underbrace{\frac{\tau}{2} \langle v_P^2 \rangle \frac{\partial U_P}{\partial r}}_{II}. \quad (8)$$

In Eq. (8) the turbulent stresses in the dispersed phase are caused by the involvement of particles into the turbulent motion of the carrier gas phase (I) and by the transport of particle momentum as a result of random motion of particles in the radial direction (II) [15].

Here, $D_{xP}$ and $D_{rP}$ are the coefficients of turbulent diffusion of particles in the axial and radial directions, defined by the random motion of particles and their entrainment by energy-carrying eddies of the gas flow [15],

$$D_{xP} = \tau(\langle u_P^2 \rangle + p_P \langle u^2 \rangle), \quad D_{rP} = \tau(\langle v_P^2 \rangle + p_P \langle v^2 \rangle).$$

The functions describing the involvement of particles into the turbulent motion of the carrier gas phase are [15]

$$q_P = 1 - \exp(-\Omega^{\varepsilon L}/\tau); \quad p_P = \Omega^{\varepsilon L}/\tau - q_P.$$

The last term in the Eq. (7) for $V_P$ simulates the effect of centrifugal force (caused by the presence of fluctuation motion of particles in the azimuthal direction) on the transport of the dispersed phase. The application of this approach suggested by Sijercic et al. [17] enables one to simplify the set of Eq. (7) for transport of the dispersed phase by abandoning the equation for transport of the azimuthal particle velocities and fluctuations.

The equations of mean-square fluctuations of the velocity of particles in the axial and radial directions have the form as in [15].

## 5. Boundary conditions

Conditions of symmetry (the absence of radial flux of momentum in the gas and dispersed phases) were preassigned on the pipe axis,

$$\frac{\partial U}{\partial r} = V = \frac{\partial U_P}{\partial r} = V_P = \frac{\partial \langle u_P^2 \rangle}{\partial r} = \frac{\partial \langle v_P^2 \rangle}{\partial r} = \frac{\partial k}{\partial r} = \frac{\partial \varepsilon}{\partial r} = 0.$$

The no-slip and impermeability conditions are valid on the wall for the gas phase velocity. The following conditions are preassigned for the kinetic turbulent energy of gas and for the rate of turbulent energy dissipation on the wall:

$$U = V = 0; \quad k = 0, \quad \varepsilon_W = \nu \left( \frac{\partial^2 k}{\partial r^2} \right)_W.$$

The boundary conditions for the averaged axial and radial velocities of the dispersed phase for a smooth wall, ignoring the interaction between particles and elements of roughness, have the following form [15]:

$$U_P = \left[ \frac{1 - w_t}{1 + w_t} \left( \frac{2}{\pi} \langle v_P^2 \rangle \right)^{1/2} - V_P \right]^{-1} \langle u_P v_P \rangle_W; \quad V_P = 0.$$

The boundary conditions for the fluctuation components of the dispersed phase velocity for a smooth wall are [15]

$$\left[ \frac{1 - w_t^2}{1 + w_t^2} \left( \frac{2}{\pi} \langle v_P^2 \rangle \right)^{1/2} - U_P \right] \langle u_P^2 \rangle = -\frac{\tau}{3} \langle v_P^2 \rangle \frac{\partial \langle u_P^2 \rangle}{\partial r};$$

$$\left[ \frac{1 - w_n^2}{1 + w_n^2} 2 \left( \frac{2}{\pi} \langle v_P^2 \rangle \right)^{1/2} - V_P \right] \langle v_P^2 \rangle = -\tau \langle v_P^2 \rangle \frac{\partial \langle v_P^2 \rangle}{\partial r};$$

Here, we take $w_t = w_n = 0.9$.

As a result of collisions with the pipe wall without slipping, a part of momentum of incident particles will lost, and the radial component of velocity of the dispersed phase changes the sign

$$U_P'' = w_t U_P'$$

$$\langle v_P^2 \rangle'' = w_n^2 \langle v_P^2 \rangle'.$$

The prime indicates the value of the parameter prior to collision with the wall surface, and the double prime – after the collision.

The initial distributions of the parameters have the form

$$U = U_1; \quad V = V_1; \quad T = T_1; \quad M_P = M_{P1}; \quad k = k_1; \quad \varepsilon = \varepsilon_1.$$

The equations for uniform initial profiles of turbulent energy $k$ and its dissipation rate $\varepsilon$ have the forms as in [18]. The turbulence intensity at the pipe inlet in the axis take $Tu_1 = 4\%$, and in the near wall region ($y_+ \leqslant 10$) – $Tu_1 = 5\%$. We assumed that the turbulence of the gas phase to be isotropic at the inlet.

## 6. Numerical realization and testing of the numerical model

The Cranck–Nicholson finite-difference scheme is used to calculate the parabolic equations. The difference scheme is of the second order of accuracy in both directions. The set of Eqs. (1)–(8) is complemented with the boundary conditions and solved by the sweep method using the Thomas algorithm (see [19]). The longitudinal pressure gradient for gas was determined using the method of Simuni [20]. The essence of the method is a constant flow rate condition for finding the longitudinal gas pressure gradient. In order to monitor the accuracy of calculations, the law of mass conservation for the gas was checked by integration over the channel cross section with known boundary conditions.

A nonuniform logarithmic computational grid was used in the radial direction. The scheme given in [19] is suitable for this problem,

$$y_{comp} = 1 - \frac{\ln\{[\beta + 1 - y/R]/[\beta - 1 + y/R]\}}{\ln[(\beta + 1)/(\beta - 1)]},$$

where $\beta$ is the parameter of crowding of points which must exceed one. In our case, $\beta = 1.03$. The distance between the

penultimate node and the wall is $y_+ = U_* y/v = 1$. In the axial direction, the grid was uniform.

All computations were performed on a $101 \times 201$ grid. Auxiliary computations were performed on a $201 \times 201$ grid. An increase in the number of nodes causes no significant changes in the calculation results.

We compared the results of our test calculations with the DNS data and with the measurement results obtained using the PIV and LDA techniques for an isothermal single-phase turbulent pipe flow of air [21], as well as with the measurement data from [22]. Satisfactory agreement is observed between the results of numerical predictions and the measurement data of [21,22] for the longitudinal mean gas velocity and distributions of mean-square velocity fluctuations.

## 7. Comparison with experimental data

The numerical calculation have been compared with experimental data obtained for the single- and two-phase turbulent pipe flow when the mean air velocity on the pipe axis was about 5.2 m/s. The Reynolds number based on the pipe diameter was $Re = 15{,}300$. The spherical glass particles used in the experiments had the nominal diameter of 50 μm (with the standard deviation 5 μm) and density $\rho_P = 2550\ \mathrm{kg/m^3}$. Measurements were performed at two particle mass loading ratios $M_P = 0.05$ and 0.35, corresponding to solid volume fractions of $\Phi = 1.6 \times 10^{-5}$ and $1.3 \times 10^{-4}$, respectively.

The axial mean velocity of air and 50 μm particles is drawn in Fig. 1. The mean velocity distributions of air for the two-phase flow (not shown on the figure) were same compared with that for unladen air flow up $M_P = 0.35$ and were no exceed limits of experimental uncertainty. The measurements show that the mean velocity of the particles larger than one of the air within the whole cross-section of the pipe. We see that the particles axial mean velocity distribution have a smoother shape as compared with one for air (for region where $0 < r/R < 0.9$). The velocity of the particles in the near wall region decreases and depends upon their mass loading. Therefore, the lager value of the particles concentration leads to the more abrupt shape of their axial mean velocity distributions. The increasing of the concentration is likely to result in an intensive momentum transfer between phases in the time-averaged motion and more closely shapes of velocity profiles of particles and carrying air.

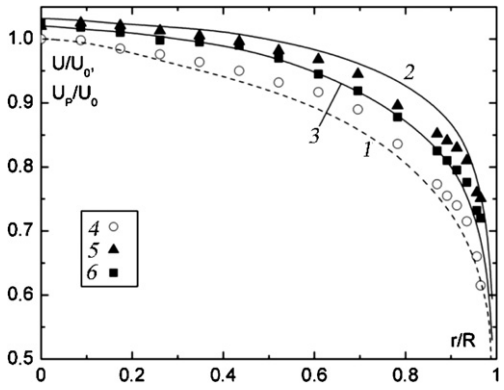


Fig. 1. Mean axial (streamwise) velocity distributions of the gas phase and the dispersed particles (glass $d = 50$ μm) at different mass loading ratio comparison between experimental (symbols) and numerical (curves) results. 1,4 – gas phase (unladen flow; $M_P = 0$); 2,5 – particles ($M_P = 0.05$); 3,6 – particles ($M_P = 0.35$).

Fig. 2 demonstrates the comparison between the prediction and experimental distributions of axial fluctuation intensities of the air $\langle u^2 \rangle / U_0$ and particles $\langle u_P^2 \rangle / U_0$ for various mass loading. The data of Fig. 2 may lead to the following inferences.

As the solid phase concentration increases, the intensity of velocity fluctuations decreases due to the involvement of particles into fluctuation motion; accordingly, a part of the turbulent energy of gas is extracted. This effect increases with the number of particles. A decrease in the intensity of fluctuations of gas velocity causes a decrease in fluctuations of the velocity of disperse phase.

The axial component of fluctuations of particle velocity increases significantly on approaching to the pipe wall. This effect is both associated with the intrinsic anisotropy of turbulence of the gas phase and caused by additional

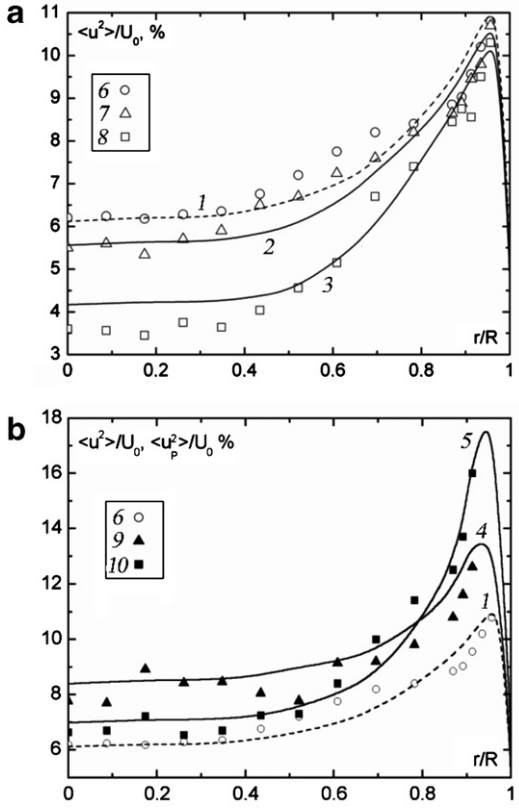


Fig. 2. Axial mean-square velocity distributions of the (a) gas phase and the (b) dispersed particles (glass $d = 50$ μm) at different mass loading ratio comparison between experimental (symbols) and numerical (curves) results. 1,6 – gas phase (unladen flow; $M_P = 0$); 2,7 – gas phase ($M_P = 0.05$); 3,8 – gas phase ($M_P = 0.35$); 4,9 – particles ($M_P = 0.05$); 5,10 – particles ($M_P = 0.35$).

generation of turbulence during the motion of particles in the field of gradient of mean axial velocity of the dispersed phase. Given the maximal value of concentration of the dispersed phase ($M_P = 0.35$), we have in these experiments and calculations $\langle u_P^2 \rangle / U_0 \approx 17\%$, which is higher than the respective characteristic for gas ($\langle u^2 \rangle / U_0 \approx 11\%$). Note that the degree of involvement of particles into the large-scale motion of the carrier phase on approaching the pipe wall decreases with increasing the Stokes number $Stk = \tau/\Omega^L$. All of the turbulent time scales decrease on approaching the wall. It is the high gradients of averaged axial gas velocity which are mainly responsible for abrupt increase in the intensity of axial fluctuations of particle velocity in the near wall region. The nonuniformity of the axial velocity profile of the carrier phase causes the nonuniformity of the profile of averaged axial velocity of particles. The particles perform intensive radial travel owing to the shift of averaged motion of gas and to their entrainment by energy-carrying eddies of the gas phase in the radial direction.

The distributions of the radial velocity fluctuations intensity of air $\langle v^2 \rangle / U_0$ and particles $\langle v_P^2 \rangle / U_0$ given in Fig. 3. The intensity of radial velocity fluctuations of particle and air for the two-phase flow is lower than one for the air of unladen flow. These facts may be interpreted as follows. The Stokes number in a large-scale fluctuation motion for the considered conditions is $Stk \approx 1$, and it follows that particles are well-involved into the large-scale fluctuation motion and extract the energy of turbulent eddies of the carrier phase. A decrease in the intensity of transverse fluctuations of the gas phase leads to a decrease in the fluctuations of small particles. The concentration of particles has a strong effect on the intensity of fluctuations of particles and gas over the entire cross section of the pipe. For example, with the concentration of disperse phase of $M_P = 0.35$, radial fluctuations decrease almost twice. For a single-phase flow ($M_P = 0$), we have $\langle v^2 \rangle / U_0 \approx 4.2\%$; for the maximal concentration of particles $\langle v_P^2 \rangle / U_0 \approx 2\%$. In the near wall region, the intensity of fluctuations of gas and particles decreases abruptly because the channel surface "prevents" the fluctuations of velocity in this direction. This is demonstrated by experimental and numerical data.

Fig. 4 display the experimental and numerical prediction data of the kinetic energy of turbulence of the unladen gas $k$ and disperse phases $k_P$ in a downward flow relatively to the value of kinetic energy of a single-phase (unladen) air flow at the pipe axis $k_{0A}$. The turbulent energy of the gas phase is estimated by the expression given in [10],

$$2k = \sum_i \langle u_i^2 \rangle = \langle u^2 \rangle + \langle v^2 \rangle + \langle w^2 \rangle \approx \langle u^2 \rangle + \langle v^2 \rangle + \frac{\langle u^2 \rangle + \langle v^2 \rangle}{2}.$$

Note that the turbulent energy of the dispersed phase is lower than the kinetic energy of gas over almost the entire cross section of the pipe except for the near wall region. The level of turbulence of the disperse phase in central region of the pipe is observed to decrease (by a factor of almost two) with increasing concentration of particles. In the near wall region, on the contrary, the fluctuation energy of particles is observed to increase (by a factor of approximately three). This fact is typical of both experimental

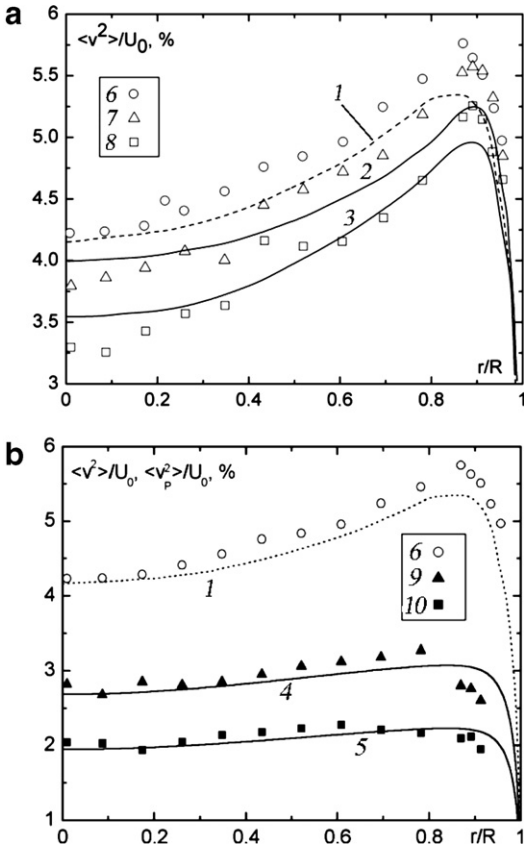


Fig. 3. Radial mean-square velocity distributions of the (a) gas phase and the (b) dispersed particles (glass $d = 50$ μm) at different mass loading ratio comparison between experimental (symbols) and numerical (curves) results. 1,6 – gas phase (unladen flow; $M_P = 0$); 2,7 – gas phase ($M_P = 0.05$); 3,8 – gas phase ($M_P = 0.35$); 4,9 – particles ($M_P = 0.05$); 5,10 – particles ($M_P = 0.35$).

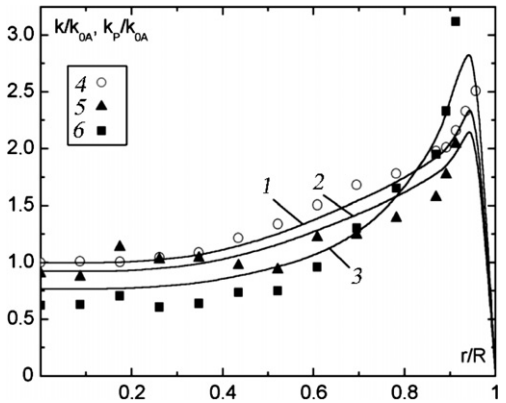


Fig. 4. Dimensionless turbulent kinetic energy distributions of the gas phase and the dispersed particles (glass $d = 50$ μm) at different mass loading ratio comparison between experimental (symbols) and numerical (curves) results. 1,4 – gas phase (unladen flow; $M_P = 0$); 2,5 – particles ($M_P = 0.05$); 3,6 – particles ($M_P = 0.35$).

and numerical data, which points to the adequacy of the model.

## 8. Results of numerical calculations and their discussion

### 8.1. Phase velocity profiles over the pipe cross section

This section gives the results of numerical calculations of isothermal turbulent heterogeneous air flow with dispersed phase of particles. The calculations were performed for the case of downward flow in a vertical pipe of diameter $2R = 50$ mm with the air velocity on the pipe axis $U_0 = 6$ m/s; the friction velocity calculated for a single-phase air flow $U_* = 0.354$ m/s; $Re = U_0 2R/v = 2 \times 10^4$; the mass loading ratio $M_P = 0.05$–$0.2$; the particle size $d = 1$–$200$ μm; $\rho_P = 1000$ kg/m$^3$ (plastic), 2550 kg/m$^3$ (glass), 3950 kg/m$^3$ (alumina), and 7800 kg/m$^3$ (iron); the dimensionless relaxation time of particles calculated for the case of Stokes mode of flow $\tau_+ = \tau U_*^2/v = 2.5 \times 10^{-2} - 10^3$ (plastic), $\tau_+ = 6.6 \times 10^{-2}$–$10^3$ (glass), $\tau_+ = 10^{-1}$–$4 \times 10^3$ (alumina), and $\tau_+ = 0.2$–$8.1 \times 10^3$ (iron). The bulk of calculations were performed for glass particles. The calculations were performed in the cross section of $x/2R = 60$, which corresponds to fully developed flow.

The radial profiles of axial mean velocity of air laden with 50 μm glass particles at various mass loading are shown in Fig. 5. Wee see, that the streamwise velocity of the gas phase is not different from those in unladen flow for all the studied cases. The observation that the statistics of gas is unaffected by presence of 50 μm glass particles for the case of $M_P = 0.05$–$0.2$ is in accordance with the above mentioned experimental observation. The profiles of mean axial air velocity of the undisturbed flow and flow laden with 50 μm glass and with 50 μm alumina particles at $M_P = 0.2$ are given in universal coordinates in Fig. 6. Note that the profiles of gas velocity in a two-phase flow differ only slightly from those in a single-phase flow, all other things being equal. This is due to the low concentration of particles and their small size.

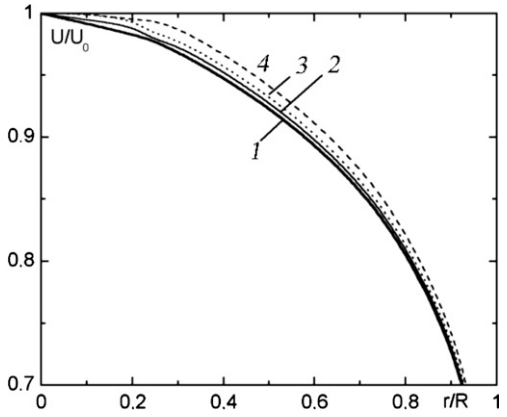


Fig. 5. Gas-phase streamwise mean velocity profiles of unladen (1) and particulate with 50 μm glass particles (2–4) air flow at different mass loading ratio. (1) $M_P = 0$; (2) 0.05; (3) 0.1; (4) 0.2.

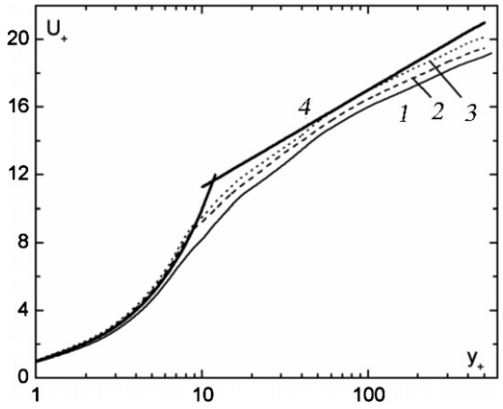


Fig. 6. Dimensionless gas-phase streamwise mean velocity profiles as a function of the dimensionless wall distance (inner scailing) of unladen $M_P = 0$ (1) and particulate $M_P = 0.2$ (2,3) air flow. (1) unladen air flow; (2) with 50 μm glass particles; (3) with 50 μm alumina particles; (4) logarithmic law of the wall.

The data given in Figs. 5 and 6 indicate that the presence of low concentration of the dispersed phase ($M_P < 0.2$) has no significant effect on the profiles of averaged velocity of the carrier gas phase. A significant effect is made by particles on the gas turbulence. These data are given in subsequent figures.

### 8.2. The effect of particles on the turbulent energy of gas

Attempts at generalizing the available experimental data on the effect of the dispersed phase on the turbulence of gas were made in [10,23–28]. Gore and Crowe [25] suggested to use the ratio of particle diameter $d$ to turbulent scale $L$ as the basic dimensionless parameter. The critical value of this parameter was shown to be $d/L \approx 0.1$. Below this value, the presence of the dispersed phase causes dissipation of turbulence; on the contrary, above this value this presence causes generation of turbulence by the particles. It was found in [26] that $d/L$ increases linearly from the channel axis to confined wall, where $d/L = 0.3$. The authors of [25–27] point out that this parameter provides an answer to the question about the direction of turbulence modulation effect (attenuation or augment) rather than to the question about the magnitude of this variation.

The variation of the value of kinetic energy of a two-phase flow on the pipe axis $k_0$ compared to the value of energy $k_{0A}$ in a single-phase (unladen) air flow is given in Fig. 7. for particles of (a) plastic, (b) glass, (c) alumina and (d) iron. The smallest particles ($d = 1$ μm) have hardly any effect on the turbulent energy of the carrier phase. They are involved into the microfluctuation motion of the gas phase which is a low-energy motion. The presence of small particles in the range of sizes treated by us leads to suppression of gas turbulence. The dissipation effect of particles increases with their mass concentration and size. According to our calculation results, the maximal suppression occurs at $d/L \approx 0.01$–$0.02$ ($d \approx 50$–$70$ μm). As the parameter $d/L$ increases, the turbulence of the carrier phase

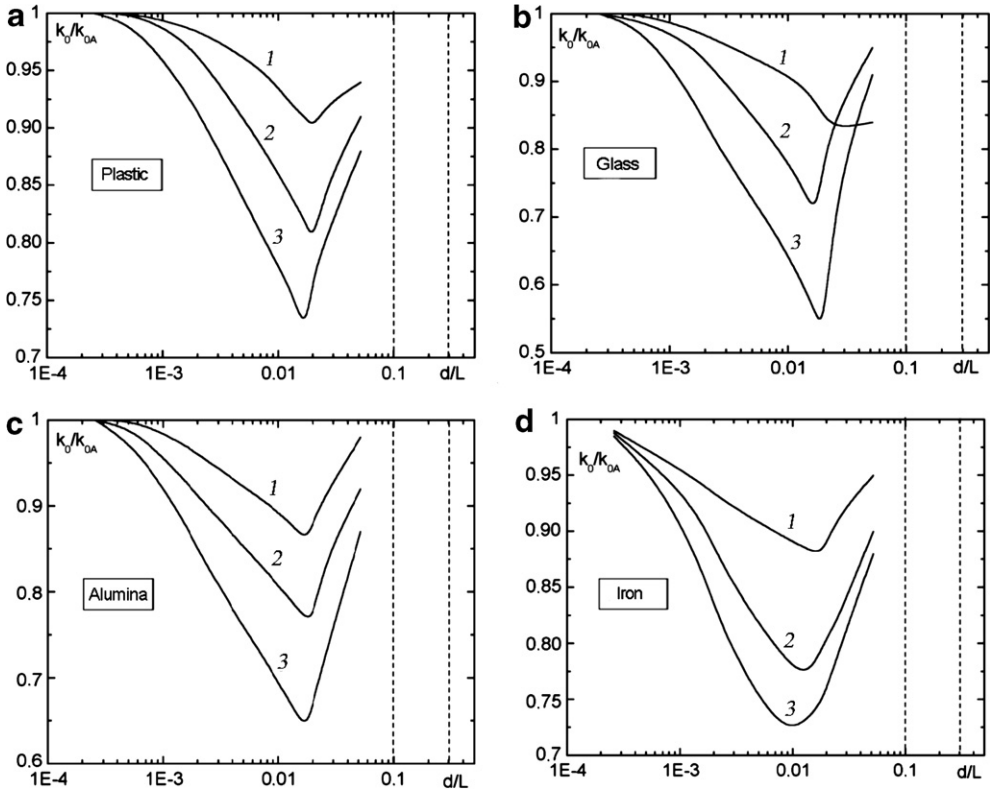


Fig. 7. Modification of gas-phase turbulent kinetic energy with particle size; $L \approx 0.14R = 3.5 \times 10^{-3}$ m; (a) plastic, (b) glass, (c) alumina, (d) iron; (1) $M_P = 0.05$, (2) 0.1, (3) 0.2. Dotted lines: $d/L = 0.1$ – according to the data of [25], $d/L = 0.3$ – according to the data of [26] for the near wall region of the pipe.

increases because larger particles of the disperse phase are involved into high-energy fluctuations with more difficulty and, accordingly, may extract less energy from the gas phase.

Fig. 8. gives data on the effect of dimensionless relaxation time of the dispersed phase on turbulence of a two-phase flow. The parameter $Z$, which characterizes the turbulent energy average over the pipe cross section, was calculated by the relation

$$Z = \frac{2}{R^2}\int_0^R \frac{k}{k_A} r\,\mathrm{d}r.$$

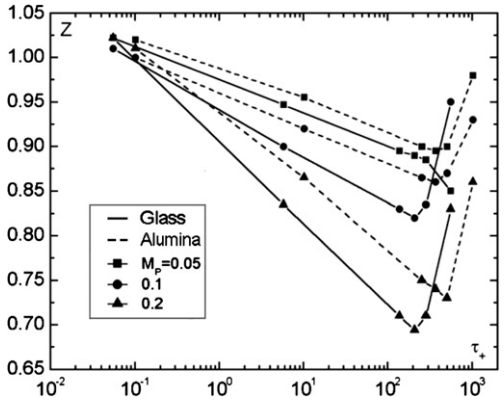


Fig. 8. The variation of the average value of gas-phase turbulent kinetic energy as a function of the relaxation time of dispersed particles at different mass loading ratio: (1) $M_P = 0.05$, (2) 0.1, (3) 0.2. Dotted – alumina particles; continuous – glass particles.

An increase in the particle size results first in a decrease in the level of gas turbulence. The decrease in the level of turbulent energy may reach approximately 30%. Then, as the particle inertia increases, the level of turbulence is observed to rise.

## 9. Conclusions

A downward turbulent air flow laden with glass solid particles has been investigated experimentally and numerically. A numerical model has been developed for calculation of turbulent gas-dispersed flows in the Eulerian approximation. The Derevich model (2002) was used to calculate the transport processes and velocity fluctuations in the dispersed phase. The turbulent characteristics of the gas phase were calculated using the Nagano–Tagawa LRN $k$–$\varepsilon$ model modified for the case of the presence of the dispersed phase. The developed numerical model enables one to fairly adequately describe the basic regularities of the processes of dynamics and mass transfer of the dispersed phase in gas-dispersed turbulent pipe flows.

Analysis of calculations under conditions of a two-phase flow with a low concentration of the dispersed phase ($M_P \leqslant 0.35$) reveals good agreement between numerical

and experimental data for the velocities and values of mean-square fluctuations of phases over the pipe cross section.

A significant anisotropy of fluctuations of particle velocity has been found. The amplitude of turbulent fluctuations of particle velocity in the axial direction is much higher than that in the radial direction. In addition to being associated with the inherent anisotropy of turbulence of the gas phase, this effect is caused by additional generation of turbulence during the motion of particles in the field of gradient of averaged axial velocity of the dispersed phase. The intensity of fluctuations of particle velocity in the axial direction may be higher than one in the case of the gas phase.

The axial and radial fluctuations of particle velocity depend strongly on the particle concentration. Loadings of solid particles into the gas flow causes a decrease in the level of turbulence of the gas phase because of the involvement of particles into fluctuation motion, as is evidenced by experimental and numerical data.

## Acknowledgements

This study was supported by a grant of the President of the Russian Federation (MK 1184.2005.8) and by the Russian Foundation for Basic Research (Grant Nos. 03-02-16251, 05-08-33586 and 05-02-16281).

## References

[1] M. Ishii, Thermo-fluid Theory of Two-Phase Flows, Eyrolles, Paris, 1975.
[2] E.P. Mednikov, Turbulent Transport and Deposition of Aerosols, Nauka, Moscow, 1981 (in Russian).
[3] G.N. Abramovich, T.A. Girshovich, S.Yu. Krasheninnikov, A.N. Sekundov, I.P. Smirnova, The Theory of Turbulent Jets, Nauka, Moscow, 1984 (in Russian).
[4] A.A. Shraiber, L.B. Gavin, V.A. Naumov, V.P. Yatsenko, Turbulent Flows in Gas Suspensions, Hemisphere, New York, 1990.
[5] R.I. Nigmatulin, Dynamics of Multiphase Media, Hemisphere, Washington, 1991.
[6] L.E. Sternin, A.A. Shraiber, Multiphase Flow with Particles, Mashinostroenie, Moscow, 1994 (in Russian).
[7] E.P. Volkov, L.I. Zaichik, V.A. Pershukov, Numerical Modeling of Combustion of Solid Fuel, Nauka, Moscow, 1994 (in Russian).
[8] D.A. Drew, S.L. Passman, Theory of Multicomponent Fluids, Springer, New York, 1998.
[9] C.T. Crowe, M. Sommerfeld, Y. Tsuji, Multiphase Flow with Droplets and Particles, CRC Press, Boca Raton, 1998.
[10] A.Yu. Varaksin, Turbulent Particle-Laden Gas Flows, Fizmatlit, Moscow, 2003 (in Russian).
[11] V.I. Terekhov, M.A. Pakhomov, The numerical modeling of the tube turbulent gas-drop flow with phase changes, Int. J. Thermal Sci. 43 (6) (2004) 595–610.
[12] V.I. Terekhov, M.A. Pakhomov, The thermal efficiency of near-wall gas-droplets screens. I. Numerical modeling, Int. J. Heat Mass Transfer 48 (2005) 1747–1759.
[13] Y. Nagano, M. Tagawa, An improved (k-$\varepsilon$) model for boundary layer flow, ASME J. Fluids Eng. 109 (1) (1990) 33–39.
[14] O. Simonin, Q. Wang, K.D. Squires, Comparison between two-fluid model predictions and large eddy simulation results in a vertical gas-solid turbulent channel flow, in: ASME Fluids Eng. Division Summer Meeting FEDSM'97, vol. 3625, 1997, pp. 1–10.
[15] I.V. Derevich, The hydrodynamics and heat transfer and mass transfer of particles under conditions of turbulent flow of gas suspension in a pipe and in an axisymmetric jet, High Temperature 40 (1) (2002) 78–91.
[16] W.S.J. Uijetterwaal, R.V.A. Oliemans, Particle dispersion and deposition in direct numerical and large eddy simulations of vertical pipe flow, Phys. Fluids A 8 (1996) 2590–2604.
[17] M. Sijercic, G. Zivkovic, S. Oka, The comparison of stochastic and diffusion models of dispersed phase in two-phase turbulent flow, in: Proceedings of the 1st International Symposium on Two-Phase Modelling and Experimentation, Pisa, Italy, 1995, pp. 375–382.
[18] K.-C. Chang, M.-J. Shyu, Revisiting the Reynolds-averaged energy equation in near-wall turbulence model, Int. J. Heat Mass Transfer 43 (2000) 665–676.
[19] D.A. Anderson, J.C. Tannehill, R.H. Pletcher, Computational Fluid Mechanics and Heat Transfer, Hemisphere, New York, 1984.
[20] L.M. Simuni, Numerical solution of a problem about non-isothermal motion of fluid in a plain pipe, J. Eng. Phys. 10 (1) (1966) 85–91.
[21] J.G.M. Eggels, F. Unger, M.H. Weiss, J. Westerweel, R.J. Adrian, R. Friedrich, F.T.M. Nieuwstadt, Fully developed pipe flow: a comparison between direct numerical simulation and experiment, J. Fluid Mech. 268 (1994) 175–209.
[22] J. Laufer, The structure of turbulence in fully developed pipe flow, NACA Technical Report TR-1174, 1954, Washington, DC, USA, pp. 1–18.
[23] P.R. Owen, Pneumatic transport, J. Fluid Mech. 39 (1969) 407–432.
[24] C.T. Crowe, Review – numerical models for dilute gas-particle flows, ASME J. Fluid Eng. 104 (1982) 297–303.
[25] R.A. Gore, C.T. Crowe, Effect of particle size on modulating turbulent intensity, Int. J. Multiphase Flow 15 (1989) 279–285.
[26] R.A. Gore, C.T. Crowe, Effect of particle size on modulating turbulent intensity: influence of radial location, ASME Turbulence Modif Dispersed Multiphase Flow 80 (1989) 31–35.
[27] C.B. Rogers, J.K. Eaton, The effect of small particles on fluid turbulence in a flat-plate turbulent boundary layer in air, Physics Fluids A 3 (1991) 928–937.
[28] S.E. Elghobashi, Particle-laden turbulent flows: direct simulation and closure models, Appl. Scient. Res. 48 (1991) 301–314.